

On the distance, reddening and progenitor of V838 Mon[☆]

U.Munari¹, A.Henden², A.Vallenari³, H.E.Bond⁴, R.L.M.Corradi⁵, L.Crause⁶, S.Desidera³, E.Giro³, P.M.Marrese¹, S.Ragaini³, A.Siviero¹, R.Sordo¹, S.Starrfield⁷, T.Tomov⁸, S.Villanova⁹, T.Zwitter¹⁰, and R.M.Wagner¹¹

¹ INAF-Osservatorio Astronomico di Padova, Sede di Asiago, I-36012 Asiago (VI), Italy

² Univ. Space Research Assoc./U. S. Naval Observatory, P. O. Box 1149, Flagstaff AZ 86002-1149, USA

³ INAF-Osservatorio Astronomico di Padova, Vicolo dell'Osservatorio 8, 35122 Padova, Italy

⁴ Space Telescope Science Institute, 3700 San Martin Drive, Baltimore, MD 21218 USA

⁵ Isaac Newton Group of Telescopes, Apartado de Correos 321, 38700 Santa Cruz de La Palma, Canarias, Spain

⁶ South African Astronomical Observatory, P.O.Box 9, Observatory 7935, South Africa

⁷ Dept. of Physics and Astronomy, Arizona State Univ., P. O. Box 871504 Tempe, AZ 85287-1504, USA

⁸ Centre for Astronomy, Nicolaus Copernicus University, ul. Gagarina 11, 87-100 Torun, Poland

⁹ Dipartimento di Astronomia, Università di Padova, 35122 Padova, Italy

¹⁰ University of Ljubljana, Department of Physics, Jadranska 19, 1000 Ljubljana, Slovenia

¹¹ Large Binocular Telescope Observatory, Univ. of Arizona, 933 North Cherry Avenue, Tucson, AZ 85721, USA

Received ... / Accepted ...

Abstract. Extensive optical and infrared photometry as well as low and high resolution spectroscopy are used as inputs in deriving robust estimates of the reddening, distance and nature of the progenitor of V838 Mon, the 2002 outbursting event that produced a most spectacular light-echo. The reddening affecting V838 Mon is found to obey the $R_V=3.1$ law and amounts to (i) $E_{B-V}=0.86$ from the interstellar NaI and KI lines, (ii) $E_{B-V}=0.88$ from the energy distribution of the B3 V component and (iii) $E_{B-V}=0.87$ from the progression of extinction along the line of sight. The adopted $E_{B-V}=0.87\pm0.01$ is also the amount required by fitting the progenitor with theoretical isochrones of appropriate metallicity. The distance is estimated from (a) the galactic kinematics of the three components of the interstellar lines, (b) the amount of extinction vs the HI column density and vs the dust emission through the whole Galaxy in that direction, from (c) spectrophotometric parallax to the B3 V companion, from (d) comparison of the observed color-magnitude diagram of field stars with 3D stellar population models of the Galaxy, from (e) comparison of theoretical isochrones with the components of the binary system in quiescence and found to be around 10 kpc. Pre-outburst optical and IR energy distributions show that the component erupting in 2002 was brighter and hotter than the B3 V companion. The best fit is obtained for a 50 000 K source, 0.5 mag brighter than the B3 V companion. The latter passed unaffected through the outburst, which implies an orbital separation wide enough to avoid mass exchange during the evolution of the binary system, and to allow a safe comparison with theoretical isochrones for single stars. Such a comparison suggests that the progenitor of the outbursting component had an initial mass $\sim 65 M_\odot$, that it was approaching the Carbon ignition stage in its core at the time it erupted in 2002 and that the age of the V838 Mon binary system is close to 4 million yr. The 2002 event is probably just a shell thermonuclear event in the outer envelope of the star.

Key words. Stars: evolution - Stars: early type - Stars: individual: V838 Mon - Stars: winds, outflows - ISM: dust, extinction - ISM: kinematics

1. Introduction

V838 Mon rose from obscurity in early January 2002, when it was discovered in outburst by Brown (2002). The unusually cool spectrum and strange light-curve helped to

Send offprint requests to: U.Munari (munari@pd.astro.it)

* Tables 3 and 4 available only in electronic form (ASCII format) at CDS via anonymous ftp to cdsarc.u-strasbg.fr (130.79.128.5) or via <http://cdsweb.u-strasbg.fr/cgi-bin/qcat?J/A+A/>

keep attention focused on the object for the next three months, until the discovery in late March by Henden, Munari and Schwartz (2002) of a light-echo rapidly developing around V838 Mon. The presence of the first Galactic light echo in ~ 70 years fostered a massive, multi-wavelength observing campaign for V838 Mon. A high spatial resolution imaging series of the light-echo expansion and evolution was collected with HST by Bond et al. (2003), recently expanded by new images secured

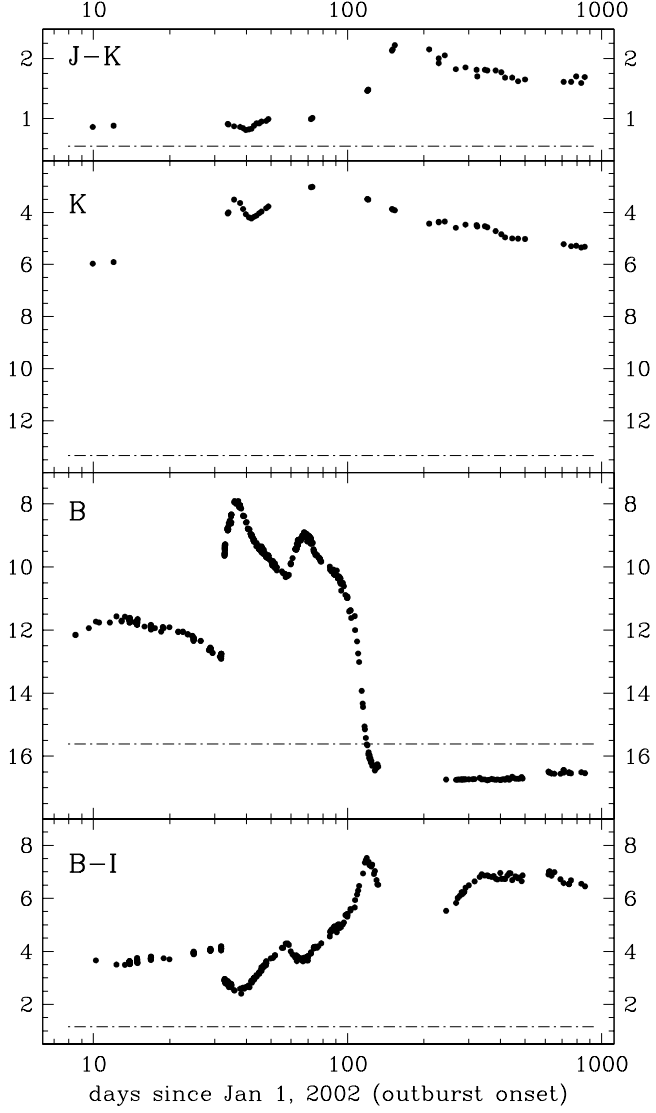


Fig. 1. Optical and IR light-curves of the outburst of V838 Mon as recorded with USNO 1.0m and 1.55m telescopes; some early-time observations come from other sources as identified in Munari et al. (2002b). The outburst onset is around Jan 1, 2002, and the first and last observations in the picture are for the dates Jan 9, 2002 and May 11, 2004, respectively. The gaps in the optical light-curves correspond to seasonal invisibility. The dotted-dashed lines give the values for the quiescence prior to the outburst.

within the Hubble Heritage Program. An account of the spectroscopic, photometric and polarimetric evolution of V838 Mon during the first season of visibility was presented by Munari et al. (2002a). A major observational constraint was the discovery by Desidera & Munari (2002) and Munari et al. (2002b) that V838 Mon is a binary system containing a normal B3V star, implying a young age and $M \geq 7 M_{\odot}$ for its outbursting companion. Over the last two years, V838 Mon has been the topic of numerous refereed papers and conference reports, with a sample given below. IR photometry and spectroscopy was pre-

Table 1. Open clusters within 5° of V838 Mon from the Lyngå (1987) catalog. θ is the angular distance in degrees from V838 Mon. Reddening and distances are taken from the Dias et al. (2002) compilation.

cluster	gal. long. ($^{\circ}$)	gal. lat. ($^{\circ}$)	θ ($^{\circ}$)	dist. (kpc)	log age (yr)	E_{B-V}
Bochum 3	218.79	+00.35	1.21	1.76	7.890	0.240
NGC 2311	217.76	-00.69	1.75	2.29	8.600	0.330
NGC 2338	219.88	+01.01	2.09			
Haffner 3	219.82	-00.01	2.29			
Berkeley 34	214.18	+01.88	3.71			
NGC 2309	219.84	-02.25	3.88	2.51	8.400	0.350
NGC 2306	219.69	-02.60	4.12			
NGC 2286	215.31	-02.27	4.16	2.90	8.883	0.170
Berkeley 77	219.36	+05.17	4.40			
NGC 2302	219.30	-03.12	4.43	1.18	7.847	0.207
NGC 2323	221.67	-01.33	4.55	0.93	8.096	0.213
NGC 2324	213.45	+03.30	4.89	3.81	8.630	0.127
Berkeley 37	217.23	+05.93	4.92			

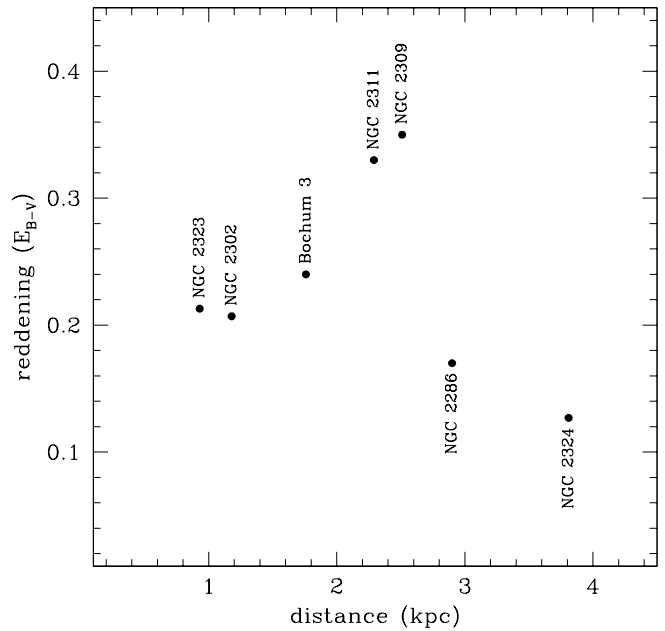


Fig. 2. Extinction as function of distance for open clusters within 5° from V838 Mon.

sented and discussed by Banerjee & Ashok (2002), Crause et al. (2003), Evans et al. (2003) and Rushton et al. (2003), optical polarimetry and spectropolarimetry by Wisniewski et al. (2003a,b) and Desidera et al. (2004), optical photometry by Kimeswenger et al. (2002), Barsukova et al. (2002), Kato (2003) and Goranskii et al. (2004), and optical spectroscopy by Munari et al. (2002a,c), Goranskii et al. (2002), Kolev et al. (2002), Osiwala et al. (2002), Kipper et al. (2004). Modeling of the outburst was presented by Retter & Marom (2003), Soker & Tyylenda (2003) and Boschi & Munari (2004), while modeling of the light-echo expansion was performed by Bond et al. (2003), Sugerman (2003) and Tyylenda (2004).

Common to many of these papers were the issues of reddening, distance and nature of the progenitor of

V838 Mon. However, none of these papers focused specifically on these topics, and limited their discussion to the derivation or adoption of approximate values based on *assumed* energy distribution of the outbursting component. The aim of the present paper is to attempt an accurate derivation of reddening and distance of V838 Mon by careful comparison of different techniques and approaches that do not involve the outbursting component, as well as to derive by comparison with theoretical models the nature and evolutionary state of V838 Mon prior to the onset of the outburst.

Optical and IR photometry used in this paper was obtained with CCD-equipped USNO Flagstaff Station (NOFS) telescopes. The $UBVR_{\text{C}}I_{\text{C}}$ data were obtained with the 1.0m telescope, the JHK'L' with the 1.55m telescope. The optical photometry is strictly tied to the Landolt (1983, 1992) system of equatorial standards, while the infrared photometry uses standard JHK' filters and differential measures with respect to local 2MASS stars. The low resolution optical spectrophotometry of V838 Mon was obtained with the AFOSC+CCD imager+spectrograph of the 1.82m telescope operated in Asiago by the Astronomical Observatory of Padova. At the same telescope we secured high resolution spectra with the Echelle+CCD spectrograph. Other high resolution spectra of V838 Mon were obtained with the Coude spectrograph+CCD of the Rozhen 2m telescope, with GIRAFFE at the 1.93m SAAO telescope, with SARG at the 3.5m TNG telescope, and with FEROS at the 2.2m ESO telescope in La Silla. Further details will be provided below where necessary.

Figure 1 presents a review of the optical and IR photometric evolution of V838 Mon, updated to the end of the third season of visibility in May 2004. With the exception of some early-time datapoints, the light-curves are entirely based on data from the USNO telescopes and therefore they are highly consistent and free from systematic effects of color transformation between different local photometric systems that would badly affect observations from different observatories of an object with such extreme colors as V838 Mon.

2. Evidence of patchy extinction

V838 Mon lies close to galactic equator ($b=+1^{\circ}$) and in the anti-center quadrant ($l=218^{\circ}$). I spite the line of sight crosses the Orion, Perseus and Outer spiral arms, inspection of the Palomar plates, of the 2MASS, IRAS, UKST- $H\alpha$ maps and the Neckel and Klare (1980) extinction charts do support an apparently smooth star counts distribution for several degrees around V838 Mon position. Therefore in principle, open clusters and field stars with accurate photometry and spectroscopic classification can be used to search for a relationship between reddening and distance in the direction of V838 Mon.

Within 5° from V838 Mon there are 13 open clusters in the catalog of Lyngå (1987). They are listed in Table 1. According to the compilation of Dias et al. (2002),

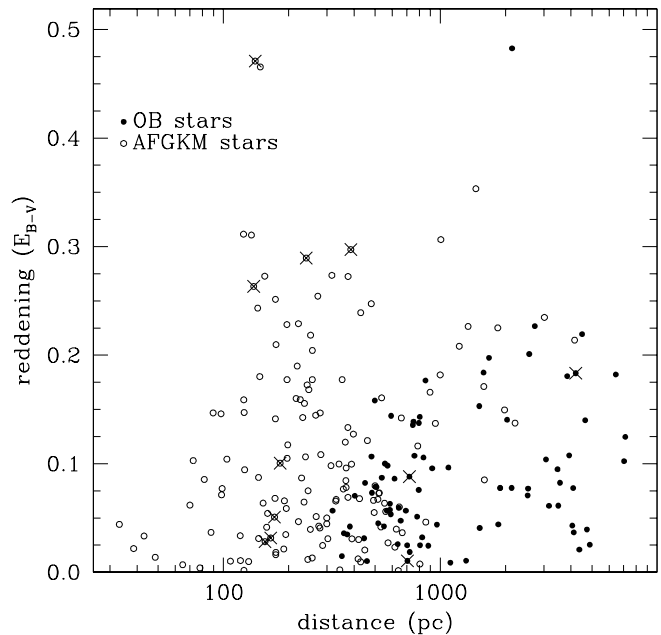


Fig. 3. The HD stars closer than 3° from V838 Mon are plotted. The crosses mark those within 0.6° from V838 Mon. Only HD stars classified by the Michigan Project and with Tycho-2 $B_{\text{T}}, V_{\text{T}}$ data are considered.

only half of them have published determinations of distance and reddening. The placing of these 7 clusters on a distance-reddening diagram (cf. Figure 2) shows a large scatter and basically no obvious trend over such angular distances.

The best source of homogeneous spectroscopic classification of field stars is the Michigan Project, which is a continuing program at the University of Michigan where all HD stars are being reclassified on the MK system, starting at the south Galactic pole, and ending at the north Galactic pole. Volume 5 (Houk & Swift 1999) covers the declination strip $-12^{\circ} \leq \delta \leq 5^{\circ}$, thus including the region around V838 Mon.

We selected all HD stars within a radius of 3° from V838 Mon and retrieved their B_{T} and V_{T} magnitudes from the Tycho-2 catalog (Høg et al. 2000). The latter were transformed into corresponding Johnson B_{J} and V_{J} following Bessell (2000) transformations. The reddening of each star was than derived by comparison with Fitzgerald (1970) intrinsic colors, and the distance computed using the absolute magnitudes of the Michigan Project scale (from N. Houk web page¹).

Figure 3 plots the distribution of HD field stars in a distance-reddening diagram. No well defined progression of the reddening with distance is evident in the figure. The amount of scatter on the diagram is much larger than justifiable in terms of measurement and classification errors, and it clearly confirms the evidence from open clusters that the reddening is very patchy over the sky area cen-

¹ <http://www.astro.lsa.umich.edu/users/hdproj/mosaicinfo/absmag.html>

Table 2. Absorption along the line of sight to V838 Mon according to the analysis of the color magnitude diagram of the field stars presented in Figures 4 and 5.

dist (kpc)	0.1	1.0	2.5	3.0	4.0	5.0	7.0	10.0
Av	0.01	0.15	0.3	0.7	1.4	1.6	2.1	2.7

tered on V838 Mon in spite of the smooth star counts distribution over the area. Even restricting to the eleven HD stars closer than 0.6° (marked by crosses in Figure 3) does not help to define a well-behaved relation between distance and reddening. This indicates that the reddening coherence area around V838 Mon has a significantly smaller radius.

3. The field stars close to V838 Mon

Noting the patchy reddening structure over degree-sized areas, we have instead focused on a much smaller angular scale in looking for a coherent relation between distance and reddening along the line of sight to V838 Mon. Deep $UBVR_CIC$ photometry of field stars within a 11×11 arcmin field centered on V838 Mon has been obtained with the NOFS 1.0m telescope. The observed color-magnitude diagrams of these field stars have then been compared to and fitted with synthetic diagrams from stellar population models of our Galaxy. The photometric data of the field stars are electronically available².

V838 Mon lies close to the galactic equator and in the general anti-center galactic direction, where stellar counts are largely dominated by the disk population. Bertelli et al. (1995) showed that the slope of the main sequence of the disk population in color-magnitude diagrams is mainly governed by the extinction along the line of sight. At any V magnitude the bluest stars on the main sequence can be interpreted as the envelope of the main sequence turnoffs of the population having absolute magnitude M_{tur} , shifted toward fainter magnitudes and redder colors by the increasing distance and corresponding extinction. Starting from an initial guess, the amount of extinction at increasing distances is adjusted (via χ^2 test on the color distribution as function of magnitude) until a satisfactory agreement between the main sequence blue edge location in the observations and in the model is reached. The distribution of observational errors is evaluated and taken into account in the process.

The Galaxy model that we used is based on the code described by Bertelli et al. (1995) and recently revised by Vallenari et al. (2000, 2004). The stars are generated according to the evolutionary model of the Galaxy, and then are distributed along the line of sight following the spatial model of the Galaxy. All stellar populations are taken into account. The generation of the synthetic population makes use of the set of the stellar tracks by Girardi et

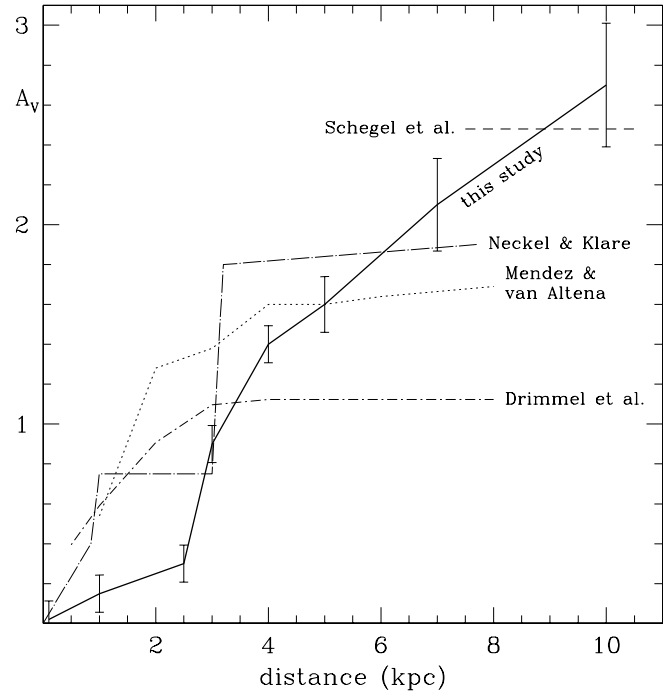


Fig. 5. Extinction along the line of sight to V838 Mon (thick and solid line) as implied by the galactic synthetic population fit in Figure 4 to the observed color-magnitude diagram of field stars. The dotted line represents the Mendez & van Altena (1998) model for the dust in the Galaxy, the short dashed-dotted line is the Drimmel et al. (2003) model, while the dashed lines give the total galactic extinction along the line of sight according to the Schlegel et al (1998) COBE maps. The long dashed-dotted line is the extinction behavior according to the Neckel & Klare (1980) maps (poorly populated at >3 kpc).

al. (2000). A double exponential mass distribution inside the thin disk is adopted having a scale length of 2500 pc and a scale height varying with the age of the population, ending at 350 pc for the oldest component. A thick disk component is included with a scale height of 800 pc. A stochastic age metallicity relation for the disk is assumed, with Z going from 0.008 to 0.03.

We performed the analysis in both $V, B-V$ and $V, V-I$ planes, with similar results. Figure 4 presents the distribution of observed and synthetic stars in the $V, V-I$ diagram, and Figure 5 gives the resulting distribution of the extinction (Av) along the line of sight. We experimented with different star formation histories in both the thin and thick galactic disks, but $Av=f(d)$ never changed by more than 0.1 mag at any point along the line of sight. The values reported in Table 4 and adopted here are those providing the best results in the χ^2 tests. The error bars in Figure 5 include both the effect of observational errors and incompleteness as well as different star formation histories in the galactic disk over the last 10 Gyr. The magnitude of turnoff stars beyond 6 kpc is at $V \geq 19$, where observational errors become significant and completeness begins to be affected. Therefore, the results in

² At http://ulisse.pd.astro.it/V838_Mon/

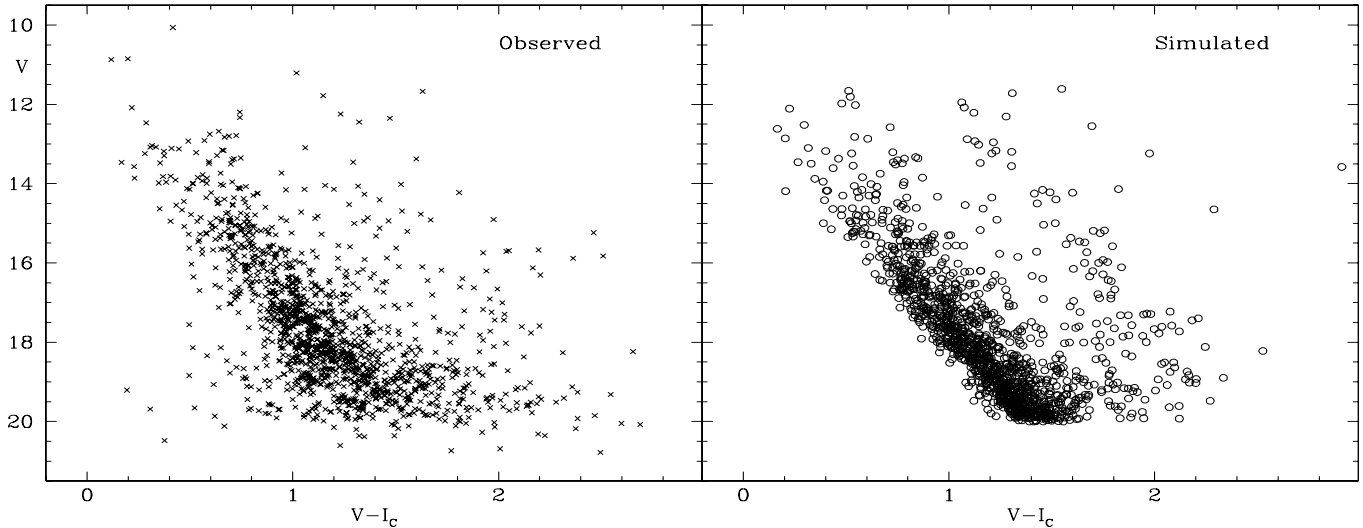


Fig. 4. The left panel plots on a V , $V - I$ diagram the stars within a 11×11 arcmin field centered on V838 Mon as observed with the NOFS 1.0m telescope. The right panel represents the fit to the observed distribution using the Padova Galaxy Model, normalized to the same number of stars (1358).

Table 4 and Figure 5 are less accurate beyond 6 kpc. To increase the accuracy at larger distances it is advisable that much deeper photometry is obtained in future observations with 8m class telescopes. Comparing the HR diagrams of field stars in different colors it is clear that a standard $R_V = A_V/E_{B-V} = 3.1$ extinction law applies.

In Figure 5 comparison is made with other $A_V = f(d)$ already presented in literature. Mendez & van Altena (1998) make use of the large-scale properties of the dust layer in the Galaxy to derive the absorption in the plane of the Galaxy. Their model indicates that a differential optical absorption of 0.5 mag kpc^{-1} is adequate to reproduce the available reddening maps in the range $2 \leq r \leq 6$ kpc. The internal uncertainties reported by Mendez & van Altena are of the order of $E_{B-V} = 0.25$, or $A_V = 0.77$ mag for a standard $A_V = 3.1 \times E_{B-V}$. Schlegel et al (1998), using the COBE-DIRBE 100 and 240 μm all sky survey, derived a map of dust emissivity, which was converted into a map proportional to dust column density and, finally, to a map of the total amount of reddening through any direction in the Galaxy. These maps are expected to suffer in accuracy close to the galactic plane, at $|b| < 5^\circ$. Drimmel et al (2003) recently presented a dimensional model of the dust distribution based on COBE-DIRBE infrared data which aims to be useful closer to the Galactic plane, since it accounts for the presence of spiral arms. As stated by Drimmel et al., regions having anomalous emission due to warm dust (like Orion or the Galactic center) are not well described by their model. Neckel & Klare (1980) extinction maps are based on observed $B - V$ colors of stars of known spectral type and luminosity class so that a spectro-photometric parallax can be estimated. Neckel & Klare data are only tentative at distances larger than 3 kpc given the paucity of data.

4. The NaI and KI interstellar lines

The interstellar lines are a powerful mean for deriving the reddening along the line of sight. Munari & Zwitter (1997) have calibrated accurate relations between reddening and equivalent width of NaI and KI interstellar lines that we apply to V838 Mon in this section.

We have secured a number of high resolution spectra during the outburst of V838 Mon which are suitable to reveal and measure the interstellar NaI and KI lines. They are summarized in Table 3 (available in electronic form only). The general appearance of interstellar lines in V838 Mon spectra is illustrated in Figure 6. There are three main components contributing to the profiles of interstellar lines. They are seen well separated in the KI line observed at a resolving power 48 000 with FEROS at the 2.2m at ESO. The two components at $+29$ and $+42$ km sec^{-1} are blended at the lower resolution of the other instruments, particularly in the case of the stronger NaI lines. For this reason these lower-resolution spectra show a narrow *red component*, at $+65.1 \text{ km sec}^{-1}$ radial velocity, and a broader *blue component*, at $+37.7 \text{ km sec}^{-1}$ radial velocity. It is worth noting that the average velocity of the two blue KI components (at $+29$ and $+42 \text{ km sec}^{-1}$) in the FEROS spectrum, weighted according to their equivalent widths, matches exactly the velocity of the blended blue component ($+37.7 \text{ km sec}^{-1}$) in the lower resolution spectra of both NaI and KI lines.

The results of the measurement of heliocentric wavelength, equivalent width and FWHM of the NaI and KI lines of spectra listed in Table 3 are given in Table 4 (available in electronic form only), separately for the blue and the red components. Their mean values and standard deviation are given in Table 5. Extensive tests on the spectra suggests that the minimal apparent changes with time traceable in Table 4 are not the result of intrinsic vari-

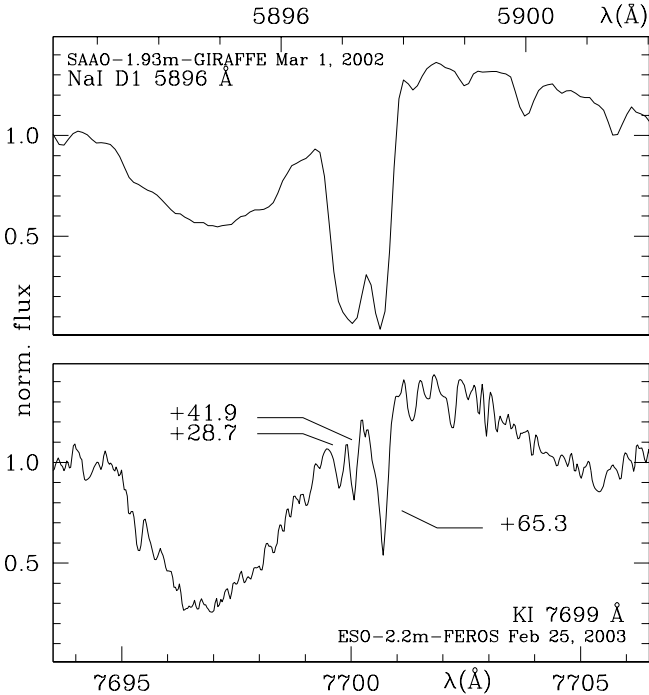


Fig. 6. Interstellar lines in the high resolution optical spectra of V838 Mon. The upper panel shows the profile of the NaI D1 line superimposed on the broad P-Cygni stellar line. The profile is composed of a narrow red component and a blue unresolved blend. The blue blend is resolved in a higher resolution FEROS observations of the KI 7699 Å line of V838 Mon on the lower panel.

Table 3. Journal of the high-resolution spectroscopic observations with the Asiago, SAAO, ESO, TNG and Rozhen telescopes (available in electronic form only).

Table 4. Results of the multi-Gaussian fitting to the NaI and KI interstellar lines in the high resolution spectra of V838 Mon listed in Table 1 (available in electronic form only).

ability of the interstellar lines themselves. Instead, they arise from the difficulty (arbitrary) in tracing the level of the underlying *continuum* in the continuously changing shape of the underlying broad stellar P-Cygni profiles (cf. Figure 6), as well as the large assortment of spectrographs - each with its own PSF - contributing to the monitoring of the interstellar lines.

The time behavior of heliocentric radial velocity, equivalent width and FWHM is plotted in Figure 7. It clearly indicates that since earliest outburst phases these values have remained constant, being unaffected by the large changes in the mass loss (amount and velocity) of V838 Mon during its active state. This indicates that the ejected material had not reached and swept away any pre-existing circumstellar material giving rise to NaI and KI absorptions, which is consistent with the absence of X-

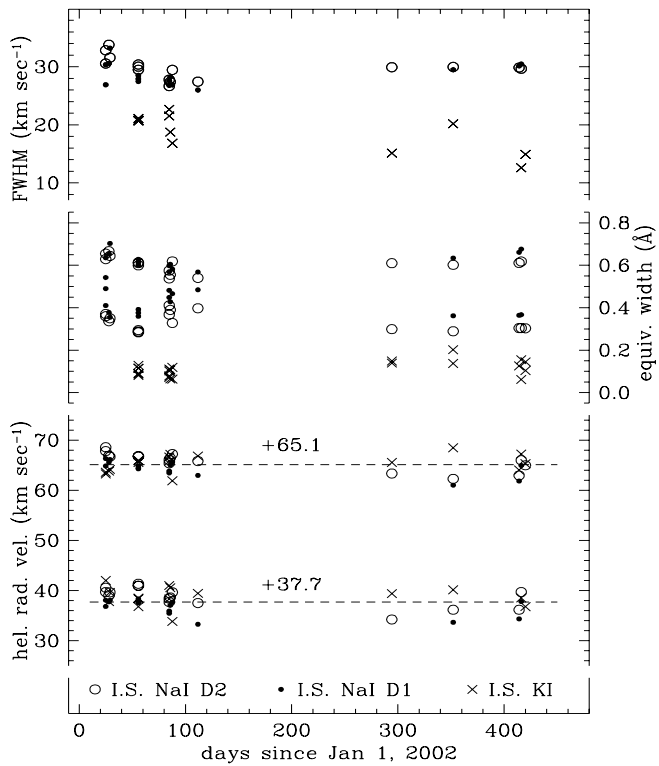


Fig. 7. Heliocentric radial velocities, equivalent widths and full width at half maximum from Table 4 of the interstellar lines as function of time since the onset of the outburst of V838 Mon around Jan 1, 2002. Their constancy suggests that the violent eruption has not interfered with possible pre-existing circumstellar material.

ray detection in Chandra observation of V838 Mon by Orio et al. 2003 and the central dust-free region described by Tylenda (2004). All three components of the interstellar lines seem truly interstellar and not circumstellar because (a) ground-based and HST images of the light-echo (Munari et al. 2002c, Bond et al. 2003, and a recent Hubble Heritage Program image) show a hole surrounding the central star, (b) the reddening from interstellar lines (cf. next section) matches that from field stars, and above all because (c) the radial velocities of the three components of the interstellar lines ($65, 42$ and 29 km sec^{-1}) precisely correspond to those of the HI complexes ($68, 43$ and 27 km sec^{-1}) observed along the line of sight to V838 Mon in the Leiden/Dwingeloo HI Survey (Hartmann & Burton 1997).

4.1. Reddening from interstellar lines

From the wavelength of maximum polarization, Desidera et al. (2004) have demonstrated how the reddening affecting V838 Mon follows the normal $R_V = A_V/E_{B-V} = 3.1$ extinction law. The same result follows from the analysis of *UBVRI* photometry of field stars in sect. 3. We can therefore safely apply to interstellar lines the Munari & Zwitter (1997) calibration for the average interstellar medium to the equivalent width of NaI and KI lines

Table 5. Mean values and standard deviations of the radial velocity (RV), full width at half maximum (Γ) and equivalent width (E.W.) of the NaI D and KI interstellar lines in the spectra of V838 Mon detailed in Table 2.

	RV	σ_{RV}	Γ	σ_{Γ}	E.W.	$\sigma_{\text{E.W.}}$
	(km sec $^{-1}$)		(km sec $^{-1}$)		(Å)	(Å)
<i>blue component</i>						
NaI D1	+38.4	1.8	29.8	1.7	0.610	0.035
NaI D2	+36.4	1.8	29.0	1.1	0.625	0.044
KI	+38.3	2.1	18.1	3.4	0.100	0.054
<i>red component</i>						
NaI D1	+65.7	1.8	18.3	1.7	0.329	0.038
NaI D2	+64.3	1.5	19.4	0.9	0.366	0.009
KI	+65.4	1.8	13.4	3.4	0.128	0.017

in Table 5. The resulting reddening is $E_{B-V}=0.86$ from KI and $E_{B-V}=0.85$ from NaI. The results are in excellent agreement between the two sets of lines. We adopt $E_{B-V}=0.86$ as the reddening indicated by the interstellar lines, giving higher weight to the results from KI lines which are still far from saturation compared to the nearly saturated NaI lines.

4.2. Distance from radial velocity of interstellar lines and the galactic rotation

Some constraints on the distance to V838 Mon can be derived by combining the observed radial velocity of interstellar material and the rotation curve of the Galaxy.

The three principal components of the interstellar absorption lines have heliocentric radial velocities of +65.1, +41.9 and +28.7 km sec $^{-1}$. In Figure 8 they are overplotted onto the rotation curve of the Galaxy from Hron (1987) and onto the velocity field in the direction of V838 Mon as derived by Brand & Blitz (1993).

The velocity of the two components at +41.9 and +28.7 km sec $^{-1}$ is compatible with a broad range of distances, while the component at +65.1 km sec $^{-1}$ supports a distance to the absorbing medium not shorter than 3 kpc, with a corresponding larger distance for V838 Mon itself. Similar lower limits to the distance to V838 Mon were derived by Wisniewski et al. (2003a) and Kipper et al. (2004) from similar kinematic arguments based on the observed velocity of interstellar lines.

5. The B3V companion

Munari et al. (2002c) commented on the fact that the $UBVR_CI_C$ light-curves of V838 Mon started to exhibit a puzzling *bluing* in $U - B$ 90 days and in $B - V$ 115 days after the outburst onset, while $V - I$ was rising to very red values, approaching those of brown dwarfs. The reason became apparent when Desidera and Munari (2002) discovered on spectra at day 274 that the contribution from the very cool outbursting component was less in the blue part of the spectrum, revealing the presence of a fainter

and hotter companion. V838 Mon was thus shown to be a binary system, and the hot companion was classified by Munari et al. (2002b) on spectra for day 300 as a B3 V star. The presence of the hot companion was confirmed on higher resolution spectra by Wagner and Starrfield (2002). The composite nature of optical spectra of V838 Mon during this phase is illustrated in the top panel of Figure 9. Later on there was an increase in the contribution of the outbursting component at shorter wavelengths, as illustrated in the bottom panel of Figure 9.

The average color of V838 Mon at the time of the naked visibility of the B3 V companion was $B-V=+0.68$ (cf. Figure 1 and Munari et al. 2002b). Comparing with the intrinsic colors of a B3 V from Fitzgerald (1970) it results in $E_{B-V}=0.88$, in excellent agreement with the results from interstellar NaI and KI lines.

The metallicity in the galactic disk at the galactocentric distance of V838 Mon is $[\text{Fe}/\text{H}]=-0.7$, about half dex lower than in the solar neighborhood (e.g. Friel et al. 2002, Hou et al. 2003). The effect on the $B-V$ color of the B3 V component in V838 Mon of such a reduction in metallicity is a very minor one, being on the Rayleigh-Jeans tail of the energy distribution of a hot star. Integrating the transmission profiles of the Landolt's B and V bands (to which our photometry is tied) to the 2500-10500 Å synthetic Kurucz spectral library of Munari et al. (2004), the net effect is just 0.007 mag.

The average V magnitude of V838 Mon at the time the V band was dominated by the radiation from the B3 V component is $V=16.05\pm0.05$. Coupled with the $E_{B-V}=0.87\pm0.01$ and an absolute magnitude $M_V=-1.70\pm0.05$ for a B3V star from Houk (2004), it implies a distance of 10 kpc to V838 Mon.

6. Combined results

6.1. Reddening

Two assumption-independent methods, the interstellar atomic absorption lines and the colors of the B3V companion, provide consistent results on the reddening affecting V838 Mon: $E_{B-V}=0.86$ and $E_{B-V}=0.88$, respectively. There is no differential extinction between the outbursting star and the B3V companion.

The same amount of reddening is derived from the modeling of the HR diagram of field stars close to V838 Mon performed in sect. 3. In fact, entering Table 2 or Figure 5 with the distance (10 kpc) to V838 Mon from the spectro-photometric parallax to the B3V companion, $E_{B-V}=0.87$ is obtained.

We therefore conclude that the extinction toward V838 Mon follows the standard $R_V = A_V/E_{B-V} = 3.1$ law and the reddening amounts to $E_{B-V}=0.87\pm0.01$.

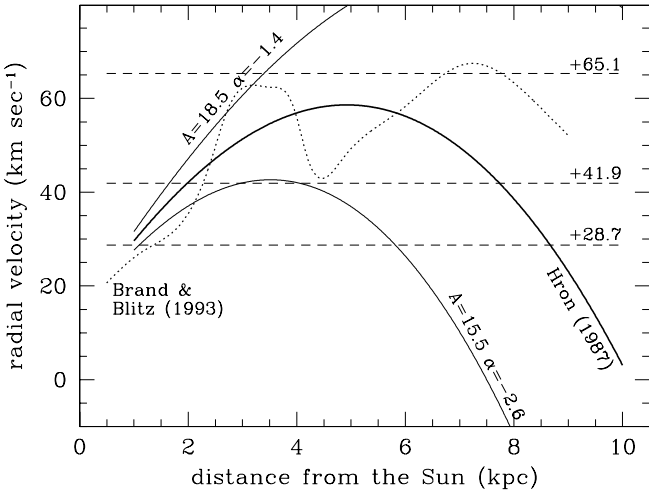


Fig. 8. The radial velocities of the three components of NaI and KI interstellar lines (+28.7, +41.9 and 65.1 km sec⁻¹) are over-plotted on the velocity field from Brand & Blitz (1993) and on the rotation curve of the Galaxy of Hron (1987). For the latter two additional curves are plotted, corresponding to the extremes of the allowed ranges for A and α parameters.

6.2. Distance

There are several and independent arguments and evidences that support a long distance scale to V838 Mon, of the order of 10 kpc.

Analysis of the high-resolution HST polarimetry images of the light-echo led Bond et al. (2003) to place a lower limit of 6 kpc to the distance of V838 Mon. Working on the same HST material, Tyrenda (2004) revised the distance to 8 ± 2 kpc.

The spectro-photometric parallax to the B3V companion derived in sect. 5 is 10 kpc. Furthermore, reversing the argument of the previous section, we can enter Table 2 or Figure 5 with the reddening $E_{B-V}=0.87$ (corresponding to $A_V=2.7$) determined from the interstellar lines and the colors of the B3V companion, obtaining the same distance of 10 kpc to V838 Mon.

Two other arguments are in favor of a large distance to V838 Mon, given its proximity to the galactic plane ($b=-3^{\circ}51'$ galactic latitude). First, we have seen above that the HI radio observations in the direction of V838 Mon reveal three components whose velocity match exactly that of the three components seen in the interstellar absorption lines. Given the fact that the radio observations integrate along the whole line of sight through the Galaxy and that no HI is seen *beyond* V838 Mon (in the sense that no corresponding interstellar lines are detected in the high-resolution spectra), it is straightforward to conclude that V838 Mon lies at great distance with most of the galactic gas, in that direction, in front of it. Second, Schlegel et al. (1998) extinction maps are based on the amount of infrared emission by the dust integrated along the whole line of sight through the Galaxy. The amount of extinction affecting V838 Mon ($E_{B-V}=0.87$ correspond-

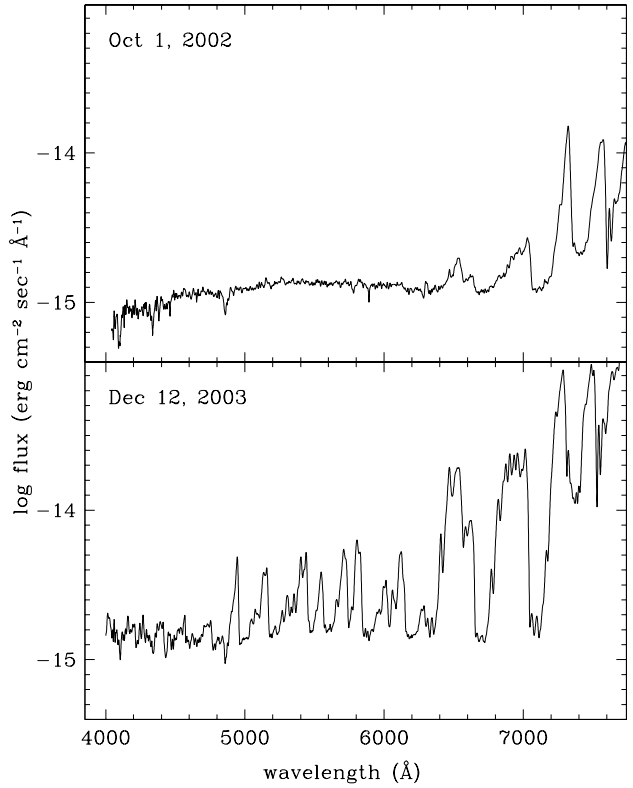


Fig. 9. Comparison between Asiago AFOSC spectra of V838 Mon taken in October 2002 and December 2003. At the earlier date the outbursting component is only visible toward the red, revealing the presence of a B3 V companion whose emission dominates the U , B and V bands at that time. The later spectrum illustrates how the emission of the outbursting component has retracted back to shorter wavelengths during the 2003/04 visibility season, a change already described in its early development by Wagner et al. (2003).

ing to $A_V=2.7$ mag) match the value of Schlegel et al. maps in that direction, supporting again the notion that V838 Mon lies at large galactocentric distances.

All these independent determinations support the conclusion that V838 Mon lies in the outer part of the disk of the Galaxy, at a distance of ~ 10 kpc from the Sun, corresponding to a galacto-centric distance of ~ 17.5 kpc and a height above the galactic plane of ~ 650 pc.

Tyrenda (2004) labeled as “naive interpretation” the early distance estimates of Munari et al. (2002a) and Kimeswenger et al. (2002) based on the first determinations of the angular expansion rate of the light-echo on early ground-based discovery images. The Munari et al. (2002a) implicit (but quite obvious) assumption was that the light-echo was originating in a circumstellar disk seen pole-on. Such an assumption was based on the fact that the NaI and KI lines were not tracing a circumstellar component, something to be expected in the case of a homogeneous spherical distribution of material centered on the object itself. It was only much later that high resolution HST imaging revealed that there is a clear void

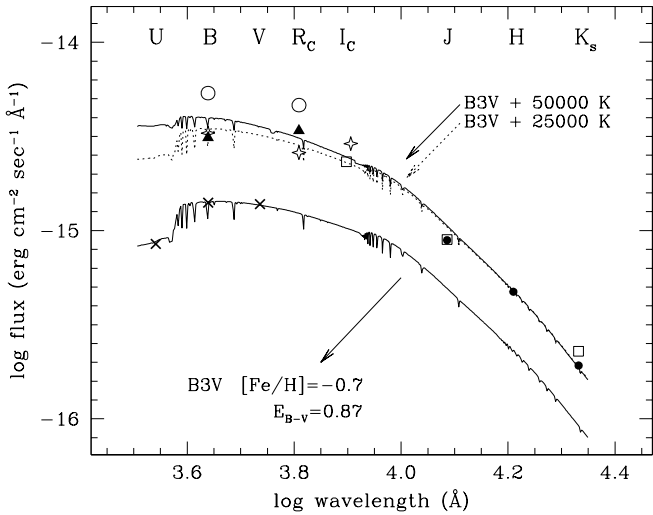


Fig. 10. The crosses represent the energy distribution of V838 Mon at the time of naked visibility of the hot companion ($V=16.05$, $B-V=+0.68$, $U-B=-0.06$) compared with a Kurucz's spectrum for a metal poor B3V star ($T_{\text{eff}}=19000$ K, $\log g=4.0$, $[\text{Fe}/\text{H}]=-0.7$) reddened by $E_{B-V}=+0.87$. The other symbols give the energy distribution of V838 Mon in quiescence: stars from Goranskii et al. (2004), triangles from Kimeswenger et al. (2002), squares from DENIS survey, dots from 2MASS survey, circles from USNO-B magnitudes re-calibrated against the comparison sequence of Munari et al. (2002), giving $B=15.28$ and $R_C=14.22$. The quiescence energy distribution is fitted with the combination of Kurucz's spectra for the B3V stars and the hotter companion.

of circumstellar material precisely along the line of sight to V838 Mon, regardless of the true 3D shape of the circumstellar dust giving rise to the light-echo. So, the now “naive” approach was reasonable at the time.

6.3. Progenitor

Figure 10 shows the energy distribution of the B3 V companion in the UBV bands ($\langle V \rangle = 16.052$, $\langle B \rangle = 16.736$, $\langle U \rangle = 16.676$ average values from USNO 1.0m photometry described in sect.1) compared with a Kurucz's synthetic spectrum (from the library of Munari et al. 2004) with parameters appropriate for the B3 V companion ($T_{\text{eff}}=19\,000$ K, $\log g=4.0$, $[\text{Fe}/\text{H}]=-0.7$). The match is excellent. In the same figure, the pre-outburst brightness of V838 Mon from various sources are plotted. In the infrared they come from the 2MASS and DENIS surveys, while the B and R_C values are estimates of the same POSS-I and SERC plates according to different authors that used different calibrations. The entries at I band (note the slightly different effective wavelengths) come from the DENIS and POSS-II surveys.

The figure clearly shows that *the progenitor of the outbursting component was brighter and hotter than the B3 V companion*. By exactly how much it depends on the still

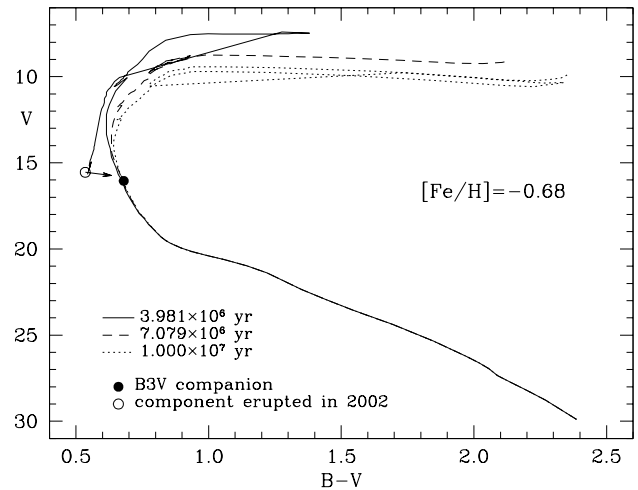


Fig. 11. Padova isochrones (from Bressan et al. 1993, Fagotto et al. 1994, Girardi et al. 2000) for $Z=0.004$ and three ages scaled to the distance (10 kpc) and reddening ($E_{B-V}=0.87$) of V838 Mon. The isochrones include the effect of mass loss and are corrected for the reddening-induced distortion described in Fiorucci & Munari (2003, their Figure 8). The open circle indicates the position of the V838 Mon component that erupted in 2002 if its temperature in quiescence was 50 000 K, and the arrow gives the shift if the temperature was 25 000 K (cf. the energy distribution fit in Figure 10).

uncertain magnitude of V838 Mon on pre-outburst photographic plates. While the brightness seems well established in the infrared by the excellent agreement of DENIS and 2MASS data, it presents a large scatter in the estimates by different authors of the same POSS and SERC plates. It is clear from Figure 10 that a careful re-evaluation of all existing pre-outburst photographic material would be beneficial in establishing the nature of V838 Mon prior to the outburst. Such a detailed analysis must first provide a perfect comparison sequence, a tight control over the plate measurement and its modeling, a careful knowledge of the exact band-pass profile of the given emulsion-filter-telescope-atmosphere combination and plate developing conditions, as well as careful application of color equation corrections.

The best fit to the V838 Mon quiescence data in Figure 10 is the B3 V plus a 50 000 K star with $V=15.55$ and $B-V=+0.535$. Both stars are equally reddened by $E_{B-V}=0.87$. The combined spectrum of the two stars is plotted in Figure 10 as a solid line. Ignoring our re-estimate of the magnitude of V838 Mon on the POSS and SERC plates listed in the caption of Figure 10, a somewhat lower temperature for the eruption progenitor can be obtained, with a lower limit of 25 000 K. The combination of the spectra of the B3 V plus a 25 000 K star with $V=15.74$ and $B-V=+0.634$ is plotted as a dotted line in Figure 10.

The location of the components of the binary system V838 Mon is compared with theoretical isochrones

in Figure 11, for the $[\text{Fe}/\text{H}] = -0.7$ metallicity appropriate to the galactocentric distance of V838 Mon and for the solar case as a matter of reference. The Padova theoretical isochrones have been scaled to a distance of 10 kpc and $E_{B-V} = 0.87$ reddening following the standard $R_V = 3.1$ extinction law. The reddening dependent deformation over the HR plane discussed and quantified by Fiorucci & Munari (2003, cf. their Figure 8) for the $UBVR_CI_C$ photometric system (Vilnius and USA reconstructions) has been applied to the isochrones in Figure 11.

As displayed by Figure 11, there is a perfect match of the $[\text{Fe}/\text{H}] = -0.7$ isochrones with the observed magnitude and colors of the B3 V component, with the progenitor of the outbursting companion lying on the isochrone for an age of 4 million yr, close to the position of the central ignition of Carbon for an initial mass of $\sim 65 M_\odot$. The progenitor lies close to the region where Wolf-Rayet stars are usually located. It would be harder to fit with theoretical evolutionary tracks the position of the progenitor of the outbursting component if its temperature would be decreased to the lower limit of 25 000 K of Figure 10, indicated by the head of the arrow in Figure 11.

We therefore conclude that the progenitor of the outbursting component of the binary system V838 Mon was hotter, brighter and born far more massive than the $7 M_\odot$ B3 V companion, of an age not far from 4 million yr. In this respect, the circumstellar scattering material giving rise to the light-echo is probably the result of the massive mass loss that such massive objects experience, where \sim half of the mass is lost during the main sequence phase. Given the location of V838 Mon in the outskirts of the Galactic disk at galactic longitude $l = 218^\circ$, the large mass and young age could sound problematic. However, young clusters and massive stars at great distances in the anti-center direction are already known. For ex., Fitzgerald & Moffat (1976) reported a distance of ~ 7 kpc for the very young cluster Ruprecht 44 ($l = 245^\circ$) rich in O and WR stars, or Marco et al. (2001) derived a distance of 6 kpc and an age of 4 Myr for the cluster NGC 1893 ($l = 173^\circ$) that harbors O5V member stars (which mass is $\sim 65 M_\odot$ according to Straižys & Kuriliené (1981) tabulation).

The outburst experienced in 2002 does not appear as the terminal event in the life of the massive progenitor, but instead more probably as a thermonuclear shell flash in the outer layers of the star as could be expected in the case of He after most of the H-rich outer envelope has been blown away by the strong wind that characterize this type of stars. A detailed analysis of the evolutionary status of the progenitor will be presented elsewhere (Munari et al., in preparation).

Acknowledgements. This work has been supported in part by Italian COFIN-2002 grant, Polish KBN Grant No. 2 P03D 019 25, and NSF and NASA grants to ASU. We would like to thank F.d'Antona and O.Straniero for useful comments.

References

Banerjee D.P.K., Ashok, N.M. 2002, A&A 395, 161

Barsukova E.A., Borisov N.V., Goranskii V.P. et al. 2002, in "Classical Nova Explosions", M. Hernanz and J. José ed.s, Am. Inst. of Physics Conf. Proc. 637, pag. 303

Bertelli, G., Bressan, A., Chiosi, C., Ng, Y.K., Ortolani, S., 1995, A&A, 301, 381

Bessell, M.S. 2000, PASP 112, 961

Bond, H.E., Henden, A., et al. 2003, Nature, 422, 405

Boschi F., Munari U. 2004, A&A 418, 869

Brand, J., Blitz, L. 1993, A&A 275, 67

Bressan A., Fagotto F., Bertelli G. et al. 1993 A&AS 100, 647

Brown N.J. 2002, IAU Circ 7785

Crause L., Lawson W.A. et al. 2003, MNRAS 341, 785

Desidera, S., Munari, U. 2002, IAUC 7982

Desidera S., Giro E., Munari U. et al. 2004, A&A 414, 591

Dias W.S., Alessi B.S. et al. 2002, A&A 389, 871

Drimmel, R., Cabrera-Lavers, A., López-Corredoira, M., 2003, A&A 409,205

Evans A., Geballe T.R., Rushton M.T. et al. 2003, MNRAS 343, 1054

Fagotto F., Bressan A. et al. 1994 A&AS 105, 29

Fiorucci, M., & Munari, U. 2003, A&A, 401, 781

Fitzgerald, M.P. 1970, A&A 4, 234

Fitzgerald, M.P., Moffat, A.F.J. 1976, A&A 50, 149

Friel, E.D., Janes, K.A., Tavarez, M. et al. 2002, AJ 124, 2693

Girardi L., Bressan A. et al. 2000, A&AS 141, 371

Goranskii, V.P., Kusakin, A.V., Metlova, N.V., et al., 2002, Astron. Letters, 28, 691

Goranskij, V.P., Shugarov, S.Yu., Barsukova, E.A., Kroll, P. 2004, IBVS 5511

Kato, T. 2003, A&A 399, 695

Kimeswenger, S., Lederle, C., Schmeja, S., Armsdorfer, B. 2002, MNRAS 336, L43

Kipper, T., Klochkova, V.G. et al. 2004, A&A 416, 1107

Kolev D., Mikolajewski M., Tomov T. et al. 2002, Collected Papers. Physics, Shumen University Press, Shumen (Bulgaria), p.147

Hartmann, L., Burton, W.B. 1997, "Atlas of Galactic Neutral Hydrogen", Cambridge Univ. Press

Henden, A., Munari, U., Schwartz, M., 2002, IAUC 7859

Høg, E., Fabricius, C. et al. 2000, A&A 355, L27

Hou, J.-L. Chang, R.-X., Chen, L. 2002, ChJAA 2, 17

Houk, N. 2004, home page of the Michigan Project: <http://www.astro.lsa.umich.edu/users/hdproj/>

Houk, N., Swift, C. 1999, Michigan catalogue of two-dimensional spectral types for the HD Stars, vol. 5, Department of Astronomy, University of Michigan

Hron, J. 1987, A&A 176, 34

Landolt, A. U. 1983, AJ 88, 439

Landolt, A. U. 1992, AJ 104, 304

Lynga, G. 1987, Catalogue of Open Cluster Data. Lund Observatory, Sweden

Marco, A., Bernabeu, G., Negueruela, I. 2001, AJ 121, 2075

Mendez, R. A., van Altena W., F., 1998, A&A 330, 910

Munari, U., Henden, A., Kiyota, S. et al. 2002a, A&A 389, L51

Munari, U., Desidera, S., Henden, A., 2002b, IAUC 8005

Munari, U., Henden, A., Corradi, R. M. L., Zwitter, T. 2002c, in "Classical Nova Explosions", M. Hernanz and J. José ed.s, Am. Inst. of Physics Conf. Proc. 637, pag. 52

Munari U., Zwitter T. 1997, A&A 318, 269

Munari, U., Sordo, R., Castelli, F., Zwitter, T. 2004, A&A, to be submitted

Neckel, Th., Klare, G 1980, A&AS 42, 251

Osiwala J.P., Mikolajewski M., Tomov T. et al. 2003, in
“Symbiotic Stars Probing Stellar Evolution”, L.Corradi et
al. ed.s, ASP Conf Ser. 303, 240

Orio, M., Starrfield, S.G., Tepedenlegliolu, E. 2004, IAUC 8110

Retter, A., Marom, A. 2003, MNRAS, 345, L25

Rushton M.T., Coulson I.M., Evans A. et al. A&A 412, 767

Schlegel, D.J., Finkbeiner, D.P., Davis, M. 1998, ApJ 500, 525

Soker, N., Tylenda, R. 2003, ApJ, 582, L105

Straižys, V., Kurilienė, G. 1981, ApSpSc 80, 353

Sugerman, B.E.K. 2003, AJ 126, 1939

Tylenda, R. 2004, A&A 414, 223

Vallenari A., Bertelli G., Schmidtobreick L., 2000, A&A 361,73

Vallenari A., Pasetto S., Bertelli G., Chiosi C., Spagna A.,
2004, A&A submitted

Wagner, R.M., Starrfield, S.G. 2002, IAUC 7992

Wagner, R.M., Schwarz, G. et al. 2003, IAUC 8202

Wisniewski J.P., Morrison N.D., Bjorkman K.S. et al. 2003a,
ApJ 588, 486

Wisniewski J.P., Bjorkman K.S., Magalhaes M. 2003b, ApJ
598, L43

Table 3. Journal of high-resolution spectroscopic observations. *HUT* = heliocentric UT date (dd/mm/yy); *HJD* = corresponding heliocentric JD (-2452000); *N* = number of spectra; *Expt* = total exposure time (in sec); *S/N* = signal-to-noise of the continuum around NaI and/or KI in the combined spectrum; *D* = dispersion; *Res* = resolving power ($\lambda/\Delta\lambda$); *slit* = aperture on the sky (in arcsec) of the spectrograph entrance slit; *lines* = interstellar lines observed.

HUT	HJD	N	Exp (sec)	S/N	D (Å/pix)	Res	slit (μ)	lines	Obs.
25.98/01/02	300.48	4	6600	121, 77	0.171, 0.225	20 000	2.0	NaI, KI	Asiago
28.91/01/02	303.41	1	1800	29, 27	0.171, 0.225	20 000	2.0	NaI, KI	Asiago
29.92/01/02	304.42	1	1800	69, 57	0.171, 0.225	20 000	2.0	NaI, KI	Asiago
25.83/02/02	331.33	3	3000	265, 210	0.171, 0.225	20 000	2.0	NaI, KI	Asiago
27.77/02/02	333.27	1	1500	90	0.100	32 000	0.8	NaI	Rozhen
1.76/03/02	335.26	1	1500	160	0.100	32 000	0.8	NaI	Rozhen
1.84/03/02	335.34	1	1800	40	0.075	39 000	2.0	NaI	SAAO
3.84/03/02	337.34	1	1800	90	0.075	39 000	2.0	NaI	SAAO
5.84/03/02	339.34	1	1800	130	0.075	39 000	2.0	NaI	SAAO
7.86/03/02	341.36	1	1800	45	0.075	39 000	2.0	NaI	SAAO
26.79/03/02	360.29	2	2400	195, 215	0.171, 0.225	20 000	2.0	NaI, KI	Asiago
27.84/03/02	361.34	1	1800	150, 195	0.171, 0.225	20 000	2.0	NaI, KI	Asiago
29.78/03/02	363.28	1	1800	205, 230	0.171, 0.225	20 000	2.0	NaI, KI	Asiago
22.82/04/02	387.32	1	1200	23, 70	0.171, 0.225	20 000	2.0	NaI, KI	Asiago
25.71/04/02	390.21	1	1200	10	0.075	39 000	2.0	NaI	SAAO
22.27/10/02	569.77	1	1600	14, 23	0.043, 0.055	29 000	1.6	NaI, KI	TNG
19.09/12/02	627.59	2	3600	15	0.225	20 000	2.0	KI	Asiago
18.94/02/03	689.44	2	3600	17	0.225	20 000	2.0	KI	Asiago
20.95/02/03	691.45	3	5400	19	0.225	20 000	2.0	KI	Asiago
25.04/02/03	695.54	5	8100	11, 33	0.030, 0.030	48 000	1.8	KI	ESO

Table 4. Results of the multi-gaussian fitting to the NaI and KI interstellar lines in the high resolution spectra of V838 Mon listed in Table 1 (rest wavelengths at 5895.923, 5889.953 and 7698.979 Å for NaI D1, D2 and KI, respectively). All wavelengths (λ) are heliocentric corrected, and the FWHMs (Γ) are corrected for the width of the instrumental PSF. Both are expressed in km sec $^{-1}$. The first two digits of the wavelengths (59 for both NaI D1 and D2, 76 or 77 for KI) are dropped for table compactness. The equivalent widths are in Å, and computed relative to a linear fit of the stellar continuum adjacent to the lines. The nomenclature *blue* and *red* components refers to the broader line at $<+37.7>$ and the narrower one at $<65.1>$ km sec $^{-1}$, respectively, that compose the profile of all interstellar lines, and that are well illustrated by the NaI D1 line at the top of Figure 1 (superimposed on the wide NaI P-Cyg stellar profile).

	NaI D1 blue comp.			NaI D1 red comp.			NaI D2 blue comp.			NaI D2 red comp.			KI blue comp.			KI red comp.		
	λ	E.W.	Γ	λ	E.W.	Γ	λ	E.W.	Γ	λ	E.W.	Γ	λ	E.W.	Γ	λ	E.W.	Γ
25.98/01/02	96.711	0.642	0.623	97.263	0.365	0.416	90.688	0.589	0.562	91.241	0.350	0.360	00.057			00.607		
28.91/01/02	96.690	0.667	0.664	97.238	0.337	0.412	90.694	0.653	0.600	91.240	0.378	0.402	99.949			00.617		
29.92/01/02	96.702	0.644	0.621	97.234	0.350	0.399	90.700	0.703	0.652	91.251	0.355	0.411	99.996			00.625		
25.83/02/02	96.731	0.608	0.590	97.236	0.289	0.321	90.696	0.615	0.549	91.220	0.376	0.389	99.951	0.086	0.535	00.667	0.119	0.343
27.77/02/02	96.634	0.602	0.589	97.147	0.289	0.322	90.614	0.634	0.579	91.151	0.362	0.391						
1.76/03/02	96.634	0.611	0.587	97.160	0.304	0.332	90.627	0.661	0.592	91.167	0.364	0.389						
1.84/03/02	96.708	0.650	0.620	97.219	0.285	0.318				91.221	0.362	0.381						
3.82/03/02	96.703	0.618	0.583	97.220	0.304	0.322	90.695	0.676	0.598	91.228	0.367	0.387						
5.84/03/02	96.698	0.617	0.582	97.218	0.306	0.321				91.217	0.369	0.375						
7.86/03/02	96.692	0.626	0.589	97.214	0.306	0.325												
26.79/03/02	96.671	0.556	0.535	97.214	0.389	0.416	90.654	0.584	0.534	91.203	0.356	0.372	99.997	0.075	0.567	00.679	0.107	0.299
27.84/03/02	96.682	0.555	0.539	97.229	0.390	0.425	90.680	0.605	0.554	91.230	0.379	0.345	00.020	0.064	0.481	00.702	0.107	0.320
29.78/03/02	96.702	0.618	0.579	97.244	0.328	0.342	90.693	0.582	0.528	91.242	0.366	0.373	99.847	0.064	0.432	00.567	0.119	0.297
22.82/04/02	96.660	0.540	0.539	97.217	0.397	0.458	90.606	0.568	0.510	91.189	0.378	0.383	99.991			00.694		
25.71/04/02	96.640	0.590	0.557	97.207	0.357	0.331							99.990	0.149	0.388	00.661	0.139	0.300
22.27/10/02	96.596	0.610	0.588	97.168	0.299	0.327							00.009	0.202	0.518	00.736	0.137	0.364
19.09/12/02																00.622	0.126	0.411
18.94/02/03																99.968	0.061	0.323
20.95/02/03																99.716	0.039	0.151
25.04/02/03																00.655	0.145	0.240
																00.054	0.065	0.232